Omori law for foreshocks and aftershocks in a realistic earthquake model

O. M. Braun[1] and M. Peyrard[2]

[1] *Institute of Physics, National Academy of Sciences of Ukraine, 46 Science Avenue, 03028 Kiev, Ukraine*
[2] *Univ Lyon, ENS de Lyon, Univ Claude Bernard, CNRS, Laboratoire de Physique, F-69342 Lyon, France*

PACS 91.30.Ab – Theory and modeling, computational seismology
PACS 91.30.Px – Earthquakes
PACS 46.55.+d – Tribology and mechanical contacts

Abstract – We study a physical model for earthquakes which extends the standard spring-block model. It is able to quantitatively describe the observations which detect differences between the statistics of foreshocks and aftershocks and the properties of main shocks. The model uses two layers to provide an intrinsic mechanism for stress relaxation and a stochastic equation to describe the contacts of crustal plates which should be treated at the scale of the elastic correlation length of the rocks and therefore result of the combined dynamics of many local contacts. The model parameters are derived from the physical properties of rocks to provide a realistic picture of the mechanisms involved in earthquakes. We show that the Omori law has different exponents for foreshocks and aftershocks, in agreement with observations. Similarly the model detects the differences in the b coefficient of the Gutenberg-Richter law for main shocks, foreshocks and aftershocks. Moreover the dynamics of the model exhibits various classes of events such as swarm of small earthquakes and major earthquakes extending over a broader fault range, suggesting that it might be the basis for further studies of the phenomena at the contact of crustal plates.

Introduction . – Large earthquakes which occur at normal hypocentral depths in brittle crustal plates are seldom isolated events. They are followed by many aftershocks, and most of them are preceded by foreshocks which could form premonitory phenomena. The empirical Omori law, first proposed in 1894 and then refined in further studies [1] expresses the decay of rate of aftershocks as

$$R(t) = \frac{K}{(t+c)^p} \tag{1}$$

where K and c are constants, p is an exponent which has typically a value near 1, and t measures the time between an aftershock and the main shock. This statistical law was first established for aftershocks but it was further realised that foreshocks too obey some systematic laws [2]. However foreshocks are not as ubiquitous as aftershocks [3], and, when they are present, their number is generally much lower than the number of aftershocks and their statistics less regular. Getting reliable data for them requires the use of a stacking method which merges many series of observations with a proper synchronisation with the time of the main shock [4, 5]. It showed that, in most of the cases, the rise of the foreshock activity before a major earthquake is also well described by the Omori law (1). However the foreshock exponent p' is generally lower than for aftershocks ($p' \approx 0.7$).

At a first glance it may seem surprising that foreshocks which correspond to the rise of activity before an earthquake, and aftershocks which are understood in terms of the redistribution of stress following the main event, can be described by the same law. This is perhaps not so surprising because the Omori law appears to be a basic law for "excitable media" and was also observed in internet traffic [6] or the activity of the blogosphere [7]. However, in the case of earthquakes, there are further fundamental questions beyond the simple validity of the Omori law. Is there a fundamental difference between the events which occur in the vicinity of a major earthquake, foreshocks and aftershocks, and the statistics of the major events themselves? Some observations point to such a difference. They show up when ones checks the Gutenberg-Richter (GR) law [8] which expresses the probability density $P(M)$ of the events of magnitude M as

$$\log P(M) = A - bM \, . \tag{2}$$

For earthquakes, the value of b is generally close to 1, but, by compiling a large number of data, Papazachos obtained a value $b \approx 0.82$ for foreshocks and $b \approx 1.31$ for aftershocks [2], suggesting that indeed the statistics of foreshocks, aftershocks are different from each other, as noticed above for the Omori law, and moreover that they also differ from the statistics of large earthquakes. One may wonder whether all these phenomena can be described within a single framework.

Several approaches have been attempted to explain the Omori law for aftershocks and foreshocks. Shaw [9] postulated a nonlinear equation for the dynamics of subcritical crack growth, which can lead to the Omori law for aftershocks, with an exponent p which depends on the postulated law. From there he could derive a law for the foreshocks, which, for $p < 1$ and in the limit of large time t, scales like the Omori law with $p' = 2p - 1$. Statistical studies, using the "epidemic-type aftershock sequence model" (ETAS) [10] can also relate the properties of foreshocks and aftershocks by assuming a "bare Omori law" which connects an aftershock with the main shock that is at its origin, and then deducing the observed laws. This approach can also justify a lower b value for the GR law of foreshocks. However, in spite of their interest, these studies are phenomenological and are not directly related to the physics of plate friction which generates earthquakes. Generic models which connect the physics of faults to earthquakes and reproduce many of the observed features have been derived from the Burridge and Knopoff spring block model [11]. The hypothesis made on the properties of the contacts are crucial. It was soon realised that contact ageing is important to get aftershocks [12]. This viewpoint evolved into a rate- and state-dependent representation of the fault constitutive properties [13–15], however the description of the GR law and the Omori law in the same framework remained problematic or required fine tuning of the parameters [16]. Moreover, to our knowledge, no model could produce a satisfactory description of both foreshocks and aftershocks, including the quantitative difference in their statistics, as well as a GR law, which also detects differences between foreshocks, aftershocks and main shocks.

Here we show that a block model with two layers to allow some stress redistribution can quantitatively describe all these phenomena in a unified framework if the properties of the contacts are modelled by a stochastic equation which results from the fluctuations of the many local contacts contributing to a macroscopic contact between plates. Moreover we pay attention to selecting parameters leading to a *realistic* model. Being one-dimensional to allow reasonably fast calculations in spite of the huge separation of the time scales that contribute to the the dynamics of earthquakes, the model cannot claim to describe the fine details of earthquakes generated by a particular fault. Nevertheless the values of the parameters can be determined from actual physical properties of the materials to make sure that the correct order of magnitude of the different physical phenomena which contribute is preserved. Moreover we show that the results do not require any fine tuning of the parameters which can vary in a rather broad range without significantly affecting the results for the Omori and GR laws.

Model. – We consider the earthquake model introduced in our earlier studies [3, 17, 18], which extends the Burridge-Knopoff model in two respects.

1) First it takes into account an intrinsic length scale, the elastic correlation length introduced in [19, 20] over which the interface responds rigidly $\lambda_c \approx a^2 Y/k$, where a is the average distance between local contacts, Y is the Young modulus of the material, and k the average elastic constants of local contacts. As a result all the local contacts situated in an area λ_c^2 move collectively as a "macro-contact". However within the macro-contact area which moves as a whole, local contacts can break or form again. Therefore the macro-contact does not obey a simple friction law. Its properties fluctuate with the dynamics of the local contacts that make it up. This behaviour can be described by a master equation [21], but its average properties can be modelled in a simpler way by a stochastic Langevin equation for the threshold force f_λ for which the macro-contact breaks [3]

$$df_\lambda/dt = B(f_\lambda) + G\xi(t) \; . \tag{3}$$

where $B(f_\lambda)$ and G are the so-called drift and stochastic force respectively and $\xi(t)$ a Gaussian random variable ($\langle \xi(t) \rangle = 0$ and $\langle \xi(t)\xi(t') \rangle = \delta(t - t')$). The idea behind the replacement of a master equation for the micro-contacts breaking and reforming by a Langeving equation is a simplifying assumption which has already been investigated in the context of friction [22]. As in the study of Brownian motion, the Gaussian δ-correlated fluctuating force summarises many short scale phenomena, the fluctuations of the micro-contacts themselves, but also external influences, such as tremors in the earth crust. To describe the ageing of the contacts we postulate

$$B(f) = \frac{f_0}{t_{\rm ageing}} \frac{(1 - f/f_0)(f/f_0)^\nu}{1 + \epsilon (f/f_0)^{\nu+2}} \tag{4}$$

and

$$G = (2/t_{\rm ageing})^{1/2} \Delta f_0 \; , \tag{5}$$

where $t_{\rm ageing}^{-1}$ determines the rate of ageing and ϵ and ν ($\nu = 2$ following [3]) are dimensionless parameters. For $\epsilon = 0$ and $\nu = 0$ the stationary solution of the Langevin equation (3) leads to a probability distribution of the contact thresholds $P(f_\lambda)$ which is a Gaussian centred at f_0, with a half-width Δf_0, which gives a physical meaning to these two model parameters. At the start of a simulation, or when a macro-contact reattaches after breaking, its breaking threshold f_λ is randomly selected with such a Gaussian distribution. Then, for $\epsilon > 0$, the initial Gaussian distribution gradually develops a power-law tail on

the side of large thresholds, i.e. the macro-contacts tend to get stronger, at a rate defined by $t_{\rm ageing}^{-1}$. As shown in [3], the factor $(f/f_0)^\nu$ introduces a "delay" in contact formation in the sense that a new-born contact, initially very weak, has a threshold that grows faster than in the asymptotic limit. The choices made for the properties of the macro-contact are consistent with the assumptions of the rate- and state-dependent representations of the fault constitutive properties [13–15] but take into account fluctuations instead of assuming a deterministic equation for the evolution of the contacts because they are based on an underlying physical model at a smaller scale [21]. This approach provides a basis to include the physical properties of the local contacts, such as the formation of chemical bonds or contact plasticity, in the properties of the macro-contacts.

2) Second, the model takes into account the internal elasticity of the crustal plates. It splits the thickness of a plate in two layers, which have some relative motions as shown in Fig. 1. The interface layer carries the macro-contacts which may attach or detach from a fixed basal plate, while the upper layer is driven by a plate moving at speed $v_{\rm drive}$. This structure allows a redistribution of the stress within the system, which occurs dynamically, while keeping this one-dimensional model much simpler than a true three-dimensional model of the elasticity of the rocks. In the spirit of the Burridge-Knopoff model, both

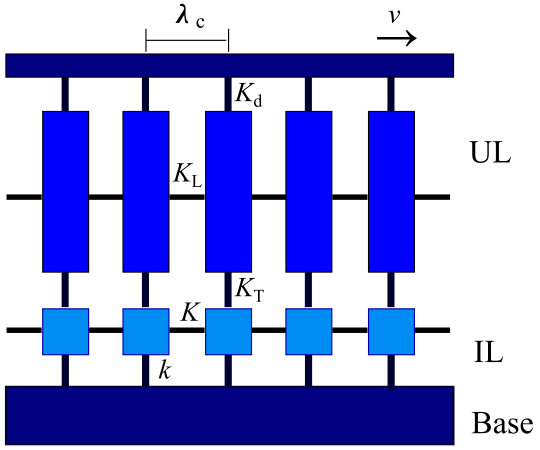

Fig. 1: Schematic picture of the model. The upper layer (UL) is split in rigid blocks of size $\lambda_c \times \lambda_c \times N_L\lambda_c$ connected by springs of elastic constant K_L. The interface layer (IL) is split in rigid blocks of size $\lambda_c \times \lambda_c \times \lambda_c$ connected by springs of elastic constant K. The UL and IL are coupled by springs of elastic constant K_T. The IL is connected with the rigid bottom block (the base) by contacts of elastic constant k, which break when the local stress exceeds a threshold value. The UL is driven with the velocity $v_{\rm drive}$ through springs of elastic constant K_d.

layers are divided in N rigid blocks. The size of a block in the direction of the fault is defined by the elastic correlation length λ_c. The interface layer, carrying the macro-contacts, is made of cubic blocks, of volume λ_c^3. The upper layer is thicker, with thickness $N_L\lambda_c$ to represent the bulk of the crustal plate. Along the fault, the blocks in both layers are connected by elastic springs representing the rock elasticity. Their elastic constant can be derived from the Young modulus of the rocks, i.e. $K = Y\lambda_c$ for the interface layer and $K_L = N_L Y\lambda_c = N_L K$ for the upper layer. The coupling constant K_T, which controls the relative motion of the two layers, is given by $K_T = Y\lambda_c/[2(1+\sigma_P)N_L]$, where σ_P is the Poisson ratio of the materials. Note that the geometry of the blocks is introduced to express the elastic constants of the model (K, K_L, K_T) as a function of the elastic properties of the material of the crustal plates. It is not an essential feature of the model. The upper layer plays the role of an elastic reservoir, where elastic energy is stored and partly released at the main shock, while the unreleased part of the elastic energy can contribute to the stress release and aftershocks. Each block i ($i = 1 \dots N$) of the interface layer is in contact with a fixed, rigid, base through a macro-contact having the breaking threshold $f_{\lambda,i}$ which evolves according to the Langevin equation (3). Its elastic constant k is related to K by $k = \kappa K$ where κ is a dimensionless parameter, chosen as $\kappa = 0.02$ to allow stick-slip at the level of the macrocontacts [22]. Simulations showed that changes in κ do not significantly alter the results if the stick-slip at the contacts is preserved. To simulate the driving of earthquakes by plate motion, the blocks of the upper layer are connected by harmonic springs of constant $K_d = K_T$ to a rigid plate moving as speed $v_{\rm drive}$.

Model parameters. Most of the model parameters can be derived from typical properties of the rocks of the crustal plates. The elastic coherence length, i.e. the length over which a piece of rock behaves as a rigid block was taken as $\lambda_c = 10\,\mathrm{m}$. As a typical Young modulus for rocks is $Y = 5\,10^{10}\,\mathrm{Pa}$ [23] we get the longitudinal coupling constant between the blocks of the interface layer as $K = Y\lambda_c = 5\,10^{11}\,\mathrm{N/m}$ and the longitudinal coupling constant between blocks of the upper layer as $K_L = N_L K = 125\,10^{11}\,\mathrm{N/m}$ if we assume a thickness of $250\,\mathrm{m} = 25\lambda_c$. The Poisson ratio was taken as $\sigma_P = 0.2$ to calculate K_T. The mass per unit volume for the rock is of the order of $\rho = 3\,10^3\,\mathrm{kg/m^3}$. These data correspond to a speed of sound in the rock $v_s = \sqrt{Y/\rho} = 4.08\,10^3\,\mathrm{m/s}$ which is a reasonable order of magnitude. With our choice $\kappa = 10^{-2}$ we get an elastic coupling constant $k = 5\,10^9\,\mathrm{N/m}$ for a macro contact. The expression of $\lambda_c = a^2 Y/k$ leads to an average distance $a = 1\,\mathrm{m}$ between local contacts, and 100 local contacts contributing to the properties of a macro-contact. The critical stress at which a solid rock breaks depends on its normal load. A typical value is of the order of 400 MPa to 1 GPa [23] so that the force that would break a macro-contact of area λ_c^2 would be in the range $4\,10^{10} - 10^{11}\,\mathrm{N}$. However most of the contact breakings do not require rock fracture but simply sliding over multiple local contacts so that the critical force f_λ at which a macro-contact breaks can be expected to be significantly lower than the rupture force. In our calculation we have

chosen $f_0 = \Delta f_0 = 10^9\,\mathrm{N/m}$ in Eqs. (4) and (5). In the simulation program that solves the Langevin equation for f_λ we set an upper bound of $5\,10^{11}\,\mathrm{N}$. However our simulations detect maxima of only $\approx 10^{11}\,\mathrm{N}$ so that this upper bound is not reached.

Numerical protocols. The model, with $N = 200$ sites and periodic boundary conditions was investigated by numerical simulations. A viscous damping with coefficient $\eta = 0.3\omega_0 = 0.3\sqrt{K_b/m}$ ($m = \rho\lambda_c^3$ being the mass of a block in the interface layer), corresponding to underdamped dynamics, has been included to describe all sources of energy losses. The mechanical equations have been solved by a 4th order Runge-Kutta algorithm while the Greenside-Helfand method [24] was used for the Langevin equations for the breaking thresholds. At each step the forces on the macro-contacts are monitored. If one of them exceeds the contact breaking threshold, the stretching of the contact drops to 0 and a new threshold is selected with a Gaussian probability distribution of average f_0 and standard deviation Δf_0. The data for this step, including the total variation of the elastic energy during the step is recorded for further analysis.

Then, in a post-simulation analysis, all *consecutive* steps in which at least one macro-contact was broken are combined in what we henceforth call an "event". The date of the event is the average time of the combined steps. The sum of all energy drops in the combined steps is called the energy E of the event, and, following [25], but measuring energies in Joules, we define the magnitude of the event as $M = (2/3)\log E$. The average displacement of all contacts that broke during this event is defined as the slip displacement δL of this event.

Typical relative velocities between plates lie in the range $35 - 160\,\mathrm{mm/year}$. A value of $100\,\mathrm{mm/year}$ amounts to about $3\,10^{-9}\,\mathrm{m/s}$. This velocity should be compared to the sound velocity in the system $v_s = 4.08\,10^3\,\mathrm{m/s}$. Therefore the typical velocities involved in the physical process that we study vary by 12 orders of magnitude. This is beyond the possibilities of numerical calculations. We decided to chose a much larger driving velocity. Our reference value is $v_{\mathrm{drive}} = 3\,10^{-3}\,\mathrm{m/s}$. This fast driving can be expected to reduce the time interval between major earthquakes by a factor 10^6. Let us check whether our results remain in line with observations. If we define a major earthquake by an elastic energy drop E which exceeds the average energy drop $\overline{E}$ of the events by $50\sigma_E$, where σ_E is the standard deviation of the energies of all recorded events, we find an average interval of 3806 s between earthquakes, i.e. $3.8\,10^9\,\mathrm{s}$ after rescaling or about 120 years. The magnitude of such earthquakes, $M = (2/3)\log E$ with E in Joules [8] is found to be $M = 8.3$. Therefore the delay of 120 years between such large earthquakes is realistic. It is important to notice that this conclusion holds even if we vary v_{drive} in the range $0.9\,10^{-3} - 9\,10^{-3}\,\mathrm{m/s}$, i.e. by one order of magnitude. The rescaled time interval between earthquakes of magnitude 8.3 was found in the range $101 - 138$ years, i.e. almost constant taking into account the expected fluctuations between different realisations.

However the need to speed-up considerably the driving has a drawback. By reducing the time interval between earthquakes to a few hours, it only allows us to monitor foreshocks and aftershocks in a small time interval around an earthquake because we have observed that *the dynamics of foreshocks and aftershocks does not scale with* v_{drive}. The results on foreshocks and aftershocks that we present in the next section are all observed within the same time interval of 350 s from the main shock although the values of v_{drive} vary by one order of magnitude. This observation time is small and is a constraint of our simulations, but on the other hand it is already an interesting result because *it shows that these shocks are true foreshocks and aftershocks.* As they do not scale with v_{drive}, they are not caused by the driving. Instead they occur due to the internal dynamics of the crustal plates, due to stress relaxation and reconfiguration.

The parameters which determine the shape of the distribution $P(f_\lambda)$ of the contact breaking thresholds are the only parameters which cannot be readily estimated from the standard properties of the rocks making crustal plates. The value of t_{ageing}, which sets the time scale for the evolution of the breaking thresholds of macrocontacts has to be evaluated in connection with the driving velocity which determines how long contacts can stick before being broken by the plate motions. In most of our calculations we have imposed $d = v_{\mathrm{drive}} \times t_{\mathrm{ageing}} = 7.5\,10^{-4}\,\mathrm{m}$. At a realistic driving velocity of $3\,10^{-9}\,\mathrm{m/s}$, this corresponds to a rescaled ageing time $t'_{\mathrm{ageing}} \approx 70\,\mathrm{hours}$, which would be an estimate of the time that a contact must stick to undergo a plastic deformation or the formation of chemical bonds which significantly alter the breaking threshold of the contact. Fortunately this is not a critical parameter. We have checked that, even if it is increased by one order of magnitude, the observable quantities, i.e. the powers p and p' of the Omori law as well as the coefficients b of the GR laws for aftershocks, foreshocks or main earthquakes are only weakly affected (see Table 1). Similarly ϵ which determines the asymmetry of the distribution i.e. the probability to get strong contacts which behave as hard points and tend to promote bigger earthquakes can be reduced from $\epsilon = 3$ to $\epsilon = 2$ without significantly changing these results (calculation 5 in Table 1).

Results. – Figure 2 shows a typical pattern of events in a short time interval containing a main shock. The intensity of the events is schematically indicated by a colour scale, from red (weak events) to blue. It illustrates the variety of the events which can be observed with the model. They correspond to different classes of earthquakes observed in nature. The weakest events (red colour in Fig. 2) tend to form sequences of similar-sized earthquakes occurring over a short period of time, similarly to swarms, which have interested seismologists for a long time [26, 27]. Stronger events (blue) are generally

more isolated but, when they reach a sufficient intensity (marked as a main shock on the figure) they occur almost simultaneously with other smaller events appearing slightly before or after them and spanning the whole fault range that we are investigating (which extends along 2 km in this calculation with $N = 200$ blocks). This leads to an average slip-displacement δL of all the macro-contacts that break which reaches a few meters and this pattern of events occurring in a very short time domain exhibits the common features of real earthquakes which generally include a sequence of motions within tens of seconds or a few minutes.

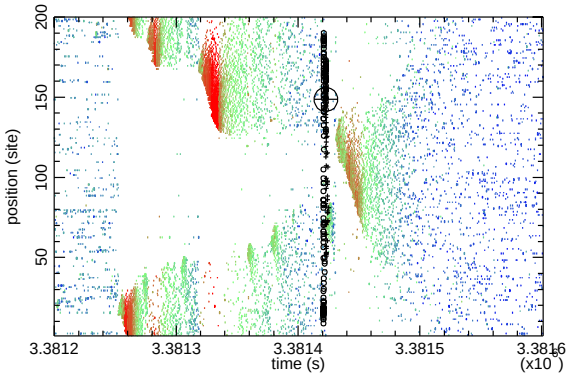

Fig. 2: Time evolution of the model during a small time interval. On this image the events are marked by points with a colour scale going from red (small energy E) to blue. A main shock is marked by a large black circle containing a cross. Black symbols (circles if they occur before the main shock, crosses if they occur after) mark events with a size exceeding the size considered for foreshocks and aftershocks. In this picture only those occurring within a few seconds of main shock are marked. They make up the line of black marks in the vicinity of the main shock. Those events actually belong to the same earthquake which typically extends over a few tens of seconds up to minutes. Therefore they are not counted in the analysis of the foreshocks and aftershocks.

Beyond this qualitative observation, for our study of foreshocks/aftershocks around such main shocks, we select the time interval $\Delta t_{\max} = 350$ s. As explained above this limited observation time is imposed by the need to use a high driving velocity in the numerical simulations. However the observation of several hundred main shocks in a simulation allows us to get good statistics to obtain meaningful results. Then we look for all moderate-size events with $E > \overline{E} + 4\sigma_E$. If there is more than one in the time domain $2.5\Delta t_{\max}$ we only keep the biggest. These events are treated as the main earthquakes (MEQ). We then make the list of smaller events ($E > \overline{E} + 0.1\sigma_E$). Those sitting within $\Delta t_{\max}$ of the main shocks are treated as foreshocks or aftershocks. Note that we do not impose any condition on the distance between a main shock and its related events because our model only describes a small piece of a fault. Remember that the size of a block

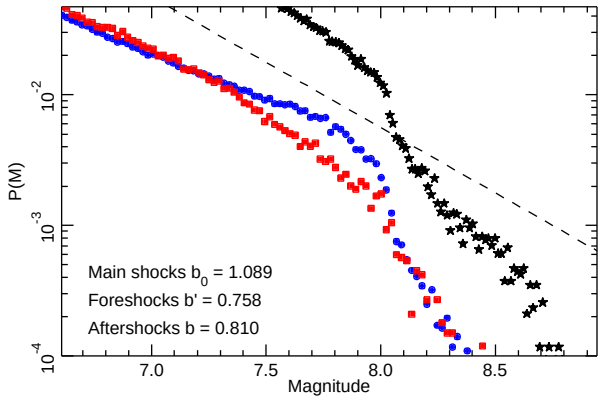

Fig. 3: Probability distribution $P(M)$ of the magnitudes of main earthquakes (MEQs) which have a magnitude above 7.5 (black stars), foreshocks (blue circles) and aftershocks (red squares) observed in calculation 1 (see Table 1). The dash black line has slope -1. For each type of event, $P(M)$ has been fitted by Eq. (2) to determine the corresponding b coefficient of the GR law (labelled b_0 for MEQs, b' for foreshocks and b for aftershocks). For large magnitudes the decay of $P(M)$ is limited by the finite simulation time. Therefore the fit is restricted to the lowest magnitude range (8 points for MEQs, 20 points for foreshocks and aftershocks which are observed in higher numbers).

is $\lambda_c = 10$ m. With $N = 200$ blocks we only investigate a piece of 2 km of a fault. We performed some calculations for $N = 500$, i.e. 5 km, but, even in this case the events are close enough to be considered as possibly related.

The statistics of the magnitudes of the main earthquakes, foreshocks, and aftershocks are plotted on Fig. 3 for one of the calculations. They are fitted by Eq. (2) to determine the b parameters separately for the MEQs (labelled b_0), foreshocks (b') and aftershocks (b). Due to the limited time of a simulation, the number of very large earthquakes ($M > 8$), which are very rare events, drastically decreases below the expected asymptotic limit of the GR law. The fit is therefore limited to lower magnitudes (see caption of Fig. 3).

To test the Omori law, our analysis uses the same stacking approach as in the studies of real earthquakes [4, 5], i.e. we collect the statistics of foreshocks and aftershocks for a large number $N_{\rm MEQ}$ of MEQs (given in table 1 for each calculation) and we determine the absolute value of the time difference t between each event and the corresponding MEQ. We divide the observation time $\Delta t_{\max}$ into 100 boxes of duration $\delta t = 3.5$ s and count the total number $n(t)$ of those events that occur within each box centred on a time difference t, in order to get the rate $R(t) = (n(t) - \overline{n})/(N_{\rm MEQ}\delta t)$ for the foreshocks and aftershocks. The value $\overline{n}$ is the average number of events in a box over the whole simulation. It corresponds to the background activity. The events in the first box ($t < \delta t$) are discarded because those events occurring in a very small interval of time from an MEQ are actually consid-

Table 1: Results of 5 test calculations with variable parameters. Calculations 1, 2, 3 test the effect of the driving velocity $v_{\rm drive}$, calculation 4 tests the effect of ϵ and calculation 5 tests the effect of an increase of $t_{\rm ageing}$ by one order of magnitude. For each calculation N_{MEQ} gives the number of main earthquakes which were analysed to get the statistics of the magnitudes and properties of the foreshocks and aftershocks.

					Omori law				GR law		
Calc	ϵ	$t'_{\rm ageing}$	$v_{\rm drive}$	$N_{\rm MEQ}$	p'	p	φ'	φ	b_0	b'	b
1	3	69.4 h	$3.0\,10^{-3}$	797	0.754	0.981	1.962	1.578	1.088	0.758	0.809
2	3	69.4 h	$0.9\,10^{-3}$	972	0.879	0.923	0.741	0.736	0.814	0.769	0.879
3	3	69.4 h	$9.0\,10^{-3}$	530	0.768	0.990	3.064	1.051	1.112	0.726	1.046
4	2	69.4 h	$3.0\,10^{-3}$	381	0.685	0.873	1.754	1.340	0.925	0.771	0.815
5	3	694 h	$3.0\,10^{-3}$	371	0.675	0.966	3.041	1.361	0.877	0.896	1.224

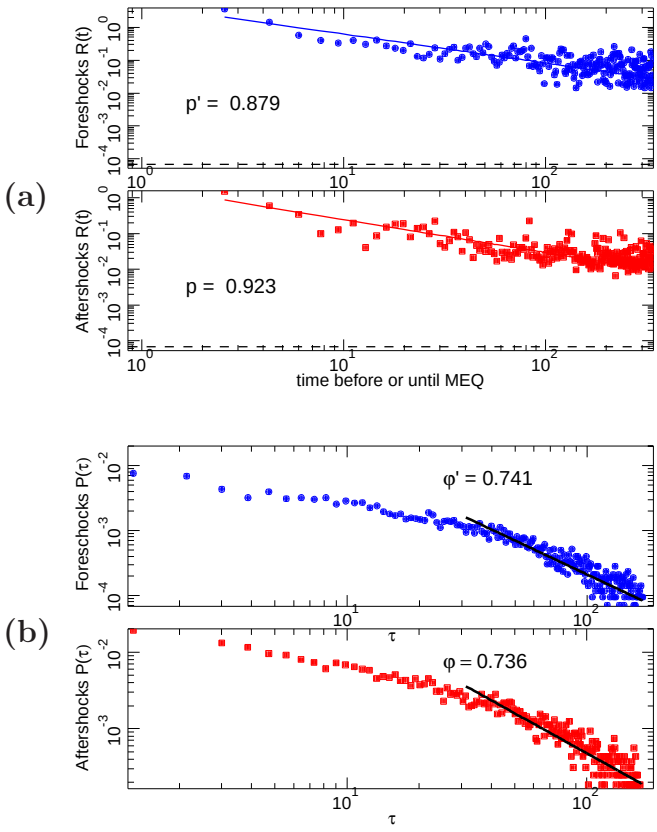

Fig. 4: (a) Test of the Omori law for calculation 2 (see Table 1). This figure shows a log – log plot of the decay rate $R(t)$ for foreshocks (blue circles) and aftershocks (red squares). On each plot the dashed black line shows the level of background activity $\overline{n}/\delta t$. (b) Probability distribution $P(\tau)$ of the time intervals between foreshocks (blue) and aftershocks (red) in the same simulation. The black lines show the power-law approximation of $P(\tau)$ for large τ.

ered as part of the main earthquake. The rate $R(t)$ for the foreshocks and aftershocks is plotted in log – log scale on Fig. 4-a, and fitted with Eq. (1) to determine the exponents p (aftershocks) or p' (foreshocks). The value of the constant c, given by the fits, is always found to be smaller than our time resolution δt and is therefore not significant. Table 1 lists the exponents p and p' for different calculations.

Figures 3 and 4 illustrate the statistical properties of many earthquakes and of their foreshock-aftershock activities for a simulation with a typical parameter set. Table 1 gives a broader and quantitative view by presenting results for a series of calculations with different parameter sets.

The first noticeable result is that, although the results rely on a spring-block model, besides the main shocks which follow the standard GR law, we detect true foreshock and aftershock activities which are clearly distinct from the main shocks. We have already pointed above that these activities around main shocks do not scale with the driving velocity $v_{\rm drive}$. This indicates that they are not governed by the external driving due to crustal plate motion. The statistics of these events confirm this feature. First, although the range in which we can study the GR law is strongly limited by the small size of the system and finite simulation time, for all parameter sets, the b' and b parameters of the GR law for foreshocks and aftershocks are different from $b_0 \approx 1$ for the main shocks. Moreover, in agreement with observations [2] b' is significantly lower than b_0 ($b' \approx 0.7$) and $b > b'$. Second, as shown in Fig. 4-a, the Omori law is very well verified, both for foreshocks and aftershocks because their rate of activity $R(t)$ is well fitted by Eq. (1). All other calculations, with other parameter sets, give the same quality of fits, demonstrating that the results are robust and not due to a fine tuning of the model parameters. This allows us to determine the exponents of the Omori law, p' for foreshocks and p for aftershocks, with a good accuracy. Here too the results clearly distinguish foreshocks and aftershocks (see Table 1). In agreement with observations [2, 4, 5] we get $p' \approx 0.7$ for foreshocks and $p \lessapprox 1$ for aftershocks.

The data that we recorded for aftershocks and foreshocks allow us to test another important property of earthquakes, the non-Markovian nature of these events [28]. This can be done by studying the time-interval distribution $P(\tau)$, where τ is the delay between two successive aftershocks (or foreshocks). The analysis shows that, in

the limit of large τ, $P(\tau)$ is a power law $P(\tau) \propto 1/\tau^{1+\varphi}$, as shown in Fig. 4-b We observe such a behaviour, for both aftershocks and foreshocks, for all set of model parameters that we investigated. However, in contrast to p and p', the values of φ (aftershocks) and φ' (foreshocks) appear to depend on the driving velocity (Table 1), possibly pointing a limitation of the simulations to study the fine structure of time-dependent properties as we cannot use realistic values of $v_{\rm drive}$. For the lowest driving speed (calculation 2 of Table 1), we have $p, p' < 1$ and $\varphi, \varphi' < 1$. In this case, a Markovian process should verify the scaling relation $p + \varphi = 1$. This relation is clearly violated by our results which show that aftershocks (and foreshocks) are non-Markovian, in agreement with the observations for actual earthquakes [28]. This is related to the large scale stress redistribution which is caused by earthquakes. With its two-layer structure our model exhibits the same behaviour.

Discussion and conclusion. – Spring-block models have been widely used to study earthquakes. Refining the friction law by introducing rate- and state-dependent relations allowed them to describe aftershocks and even foreshocks, at the expense of parameter fine-tuning [16]. We have shown that an extended model based on physical ideas introducing two layers to allow stress redistribution and a stochastic model for the complex contacts between plates, which actually involve the dynamics of many local contacts over the elastic correlation length for which the interface responds rigidly, allows to go much further in the analysis of observations. Most of the model parameters can be derived from the physics of the crustal plates, and the results are robust with respect to large variations of the few parameters that cannot be readily quantitatively estimated. The model exhibits true foreshock/aftershock activities which are distinct from the main earthquakes. Moreover the statistical analysis leads to GR laws and Omori laws which are in rather good quantitative agreement with observations, even for subtle effects such as the different properties of foreshocks and aftershocks.

Being one-dimensional the model cannot claim to quantitatively describe all phenomena involved in real earthquakes, but it is nevertheless able to exhibit different classes of events, such as swarms of small-intensity earthquakes which had only been observed in much more elaborate models [29]. Therefore this model should also allow a further understanding of some earthquake properties, beyond the Omori and GR laws on which we focused our attention in the present study.

* * *

This work was partially supported by CNRS-Ukraine PICS grant No. 151539. O.B. was supported in part by COST Action MP1303.

REFERENCES

[1] Utsu T., Ogata Y. and Matsu'ura R., *J. Phys. Earth*, **43** (1995) 1.
[2] Papazachos B.C., *Tectonophysics*, **28** (1975) 213.
[3] Braun O.M. and Peyrard M., *Geophys. J. Int.*, **213** (2018) 676.
[4] Maeda K., *Pure appl. geophys.*, **155** (1999) 381.
[5] Peng Zhigang, Vidale J.E., Ishii M. and Helmstetter A., *J. Geophys. Res.*, **112** (2007) B03306.
[6] Abe S. and Suzuki N., *Europhys. Lett.*, **61** (2003) 852.
[7] Klimek P., Bayer W. and Thurner S., *Physica A*, **390** (2011) 3870.
[8] Gutenberg B. and Richter C.F., *Seismicity of the earth* (Princeton Press) 1954
[9] Shaw B.E., *Geophys. Res. Lett.*, **20** (1993) 907.
[10] Helmstetter A., Sornette D. and Grasso J.-R., *J. Geophys. Res.*, **108** (2003) 2046.
[11] Burridge R. and Knopoff L., *Bull. Seismol. Soc. Am.*, **57** (1967) 341.
[12] Dieterich J.H., *J. Geophys. Res.*, **77** (1972) 3771.
[13] Ruina A., *J. Geophys. Res.: Solid Earth*, **88** (1983) 10359.
[14] Marone C., *Ann. Rev. Earth. Planet. Sci.*, **26** (1988) 643.
[15] Dieterich J.H., *J. Geophys. Res.: Solid Earth*, **99** (1994) 2601.
[16] Jagla E.A. and Kolton A.B., *J. Geophys. Res.: Solid Earth*, **115** (2010) B05312.
[17] Braun O.M. and Tosatti E., *Phys. Rev. E*, **90** (2014) 032403.
[18] Braun O.M. and Scheibert J., *Tribology Letters*, **56** (2014) 553.
[19] Caroli C. and Nozières Ph., *Eur. Phys. J. B*, **4** (1998) 233.
[20] Braun O.M., Peyrard M., Stryzheus D.V. and Tosatti E., *Tribology Letters*, **48** (2012) 11.
[21] Braun O.M. and Peyrard M., *Phys. Rev. Lett.*, **100** (2008) 125501.
[22] Braun O.M., *EPL*, **109** (2015) 48004.
[23] Ohnaka M., *Rock Failure and Earthquakes* (Cambridge University Press, Cambridge) 2013
[24] Greenside H.S. and Helfand E, *The Bell Technical Journal*, **60** (1981) 1927.
[25] Hanks T.C. and Kanamori H., *J. Geophys. Res. B*, **84** (1979) 2348.
[26] McGuire J.J., *Nature Geoscience*, **12** (2019) 82.
[27] Roland E. and McGuire J.J., *Geophys. J. Int.*, **178** (2009) 1677.
[28] Abe S. and Suzuki N., *Physica A*, **388** (2009) 1917.
[29] Hainzl S., *J. Geophys. Res.*, **159** (2004) 1090.